Phenol as Proton Shuttle and Buffer for Lithium-mediated Ammonia Electrosynthesis

Ib Chorkendorff

ibchork@fysik.dtu.dk

Technical University of Denmark https://orcid.org/0000-0003-2738-0325

Xianbiao Fu

Technical University of Denmark https://orcid.org/0000-0001-5172-3354

Aoni Xu

Technical University of Denmark

Jakob B. Pedersen

Technical University of Denmark

Shaofeng Li

DTU

Rokas Sažinas

Technical University of Denmark

Yuanyuan Zhou

Technical University of Denmark

Suzanne (Zamany) Andersen

Technical University of Denmark

Saccoccio Saccoccio

Technical University of Denmark

Niklas H. Deissler

Technical University of Denmark https://orcid.org/0000-0001-9117-5030

Jon Mygind

Technical University of Denmark

Jakob Kibsgaard

Technical University of Denmark

Peter Vesborg

DTU Technical University of Denmark https://orcid.org/0000-0002-3761-4212

Jens Nørskov

DTU https://orcid.org/0000-0002-4427-7728

Article

Keywords:

Posted Date: July 26th, 2023

DOI: https://doi.org/10.21203/rs.3.rs-3166795/v1

Additional Declarations: There is **NO** Competing Interest.

Version of Record: A version of this preprint was published at Nature Communications on March 18th, 2024. See the published version at https://doi.org/10.1038/s41467-024-46803-w.

Phenol as Proton Shuttle and Buffer for Lithium-mediated Ammonia Electrosynthesis

Xianbiao Fu[†], Aoni Xu[†], Jakob B. Pedersen, Shaofeng Li, Rokas Sažinas, Yuanyuan Zhou, Suzanne Z. Andersen, Mattia Saccoccio, Niklas H. Deissler, Jon Bjarke Valbæk Mygind, Jakob Kibsgaard, Peter C. K. Vesborg, Jens K. Nørskov[*], Ib Chorkendorff[*]

Department of Physics, Technical University of Denmark, Kongens Lyngby, Denmark
†These authors contributed equally to this work

*Corresponding author. Email: jkno@dtu.dk (J.K.N.), ibchork@fysik.dtu.dk (I.C.)

Abstract

Ammonia is a crucial component in the production of fertilizers and various nitrogen-based compounds. Now, the lithium-mediated nitrogen reduction reaction (Li-NRR) has emerged as a promising approach for ammonia synthesis at ambient conditions. The proton shuttle plays a critical role in the proton transfer process during Li-NRR. However, the structure-activity relationship and design principles for effective proton shuttles have not yet been established in practical Li-NRR systems. Here, we propose a general procedure for verifying a true proton shuttle and established design principles for effective proton shuttles. We systematically evaluate several classes of proton shuttles in a continuous-flow reactor with hydrogen oxidation at the anode. Among the tested proton shuttles, phenol exhibits the highest Faradaic efficiency of 72 ± 3% towards ammonia, surpassing that of ethanol, which has been commonly used so far. Experimental investigations including operando isotope-labelled mass spectrometry proved the proton-shuttling capability of phenol. Further mass transport modeling sheds light on the mechanism.

Ammonia (NH_3) synthesis has shaped our modern civilization and will continue to play a key role in our planet's future, owing to ammonia being a feedstock to produce fertilizers, polymers, pharmaceuticals, and fine chemicals[1-3]. Currently, industrial ammonia synthesis is the Haber-Bosch process using iron-based catalysts under high temperatures and pressures (*i.e.*, 350 -450 ^oC and 100-200 bar), which contributes ~1.3% of global carbon dioxide emissions[4]. The Haber-Bosch process demands very high pressure, and entails significant capital investment and large, centralized plants, whereas the utilization of fertilizers is characterized by decentralization. As renewable electricity prices decline, electrochemical ammonia synthesis offers the potential for decentralized fertilizer production in compact devices that can be coupled with decentralized renewable electricity sources. This development has the potential to reduce the cost of fertilizers in remote regions that lack efficient transportation networks by eliminating the need for extensive transportation.[3] Tremendous efforts have been made to achieve electrochemical ammonia synthesis by using nitrogen (N_2) and water as feedstock and powered by renewable energy under ambient conditions[5-8]. To date, the most promising and reliable method of electrochemical ammonia synthesis is lithium-mediated nitrogen reduction reaction (Li-NRR) in nonaqueous electrolytes[9,10]. In 1930, Fichter *et al.* first explored the Li-NRR in an alcoholic solution of lithium halide[11]. The Li-NRR was further investigated by Tsuneto *et al.* using tetrahydrofuran (THF) with small amounts of ethanol (EtOH) as an electrolyte in 1993 and 1994[12,13]. Our group proposed a rigorous procedure with gas purification and quantitative isotope measurements to avoid false positives, which validated that the produced ammonia during the Li-NRR process was from N_2 reduction[9]. Since then, many strategies have been proposed to improve the performance of the Li-NRR system[4, 14-28]. Recently, high current density (-1 A cm_{geo}^{-2}) and faradaic efficiency (FE) towards ammonia (close to 100%) have been achieved in a pressurized batch-type reactor (15 bar

or 20 bar), but the solvent was oxidized to generate the necessary protons [26,27]. In general, most Li-NRR investigations published so far use a sacrificial solvent as a proton source[28]. In order to achieve practical viability, however, the protons must come from hydrogen (or water), so the hydrogen oxidation reaction (HOR) has been proposed as the anode reaction of the Li-NRR system to provide a sustainable hydrogen source[15,28]. Very recently, we achieved an ammonia FE of 61% in a continuous-flow reactor by employing nitrogen reduction coupled with HOR at ambient pressure and temperature[28]. Isotope-labeling studies using operando mass spectrometry revealed the hydrogen implemented in the ammonia is indeed coming from the anode via H_2 oxidation[28].

Generally, the Li-NRR process contains three steps to produce ammonia. Firstly, the Li^+ is electrochemically reduced into metallic Li on the cathode and is capable of dissociating N_2 to generate lithium surface nitride, which is protonated by a proton shuttle (*e.g.*, EtOH) to release ammonia and Li^+ to repeat the cycle[4,29]. The proton shuttle can have a decisive impact on the performance of the Li-NRR system. The proton shuttle screening was first investigated by Krishnamurthy *et al*. in the two-compartment electrochemical cell with a polyporous Daramic separator after passing 7.2 C of charge (6 mins)[21]. They found that 1-butanol was the most effective proton shuttle (FE of 15.6%) and phenol (PhOH) was an inactive proton shuttle (FE of 0%). The Kamlet-Taft parameters were used as descriptors to interpret the activity toward ammonia production. Later work explained that the effect of the proton shuttle on the performance was due to the proton shuttle changing the properties of the solid electrolyte interphase (SEI)[22]. Suryanto *et al.* found the phosphonium-based salts ($[P_{6,6,6,14}][eFAP]$) can re-protonate the phosphonium cation by reacting with acetic acid but not checked in the real Li-NRR process[17]. The proton shuttles were again screened by using lithium bis(trifluoromethylsulfonyl)imide (LiTFSI) electrolyte in the batch-type reactor (15 bar)[23]. The above-mentioned works on proton shuttle

screening tried to correlate the acid dissociation constant (pK_a, values in water) of proton shuttles with the performance of the Li-NRR, but the correlation was not strong[21,23]. So far, there are no experimental studies to screen proton shuttles in the practical Li-NRR process with HOR at the anode side. Therefore, whether the proton shuttle can actually transport the protons generated by HOR to the cathode to participate in ammonia production is still unknown. Although some progress has been made, the structure-activity relationship and the role of proton shuttles in the Li-NRR process are still lacking a good understanding.

In our recent work, we successfully achieved electrochemical ammonia synthesis by coupling N_2 reduction with HOR in the continuous-flow reactor and demonstrated the hydrogen in the produced ammonia is from HOR[28]. In this work, proton shuttle screening experiments were performed in a continuous-flow reactor in the presence of HOR at the anode after passing a charge of 700 C (over 2.5 h). We proposed a general procedure on how to prove the proton shuttle works and established design principles for effective proton shuttles in the practical Li-NRR process. Contrary to previous works[21,22], we find that PhOH can achieve the highest FE of 72 ± 3% at ambient pressure and temperature, which exceeds the state-of-the-art EtOH. Although the earlier work achieved a FE of almost 100% at 15 bar pressure in the batch-typed reactor, this system relies on the sacrificial agent for providing protons.[26] Theoretical mass transport modeling clarifies the dependence of the Li-NRR performance on the pK_a (values in THF) and diffusion coefficient of proton shuttles. Our finds offer a comprehensive framework for the rational design principles of efficient proton shuttles in Li-mediated ammonia synthesis.

Results and discussion

Proton shuttle screening in a continuous-flow reactor

The Li-NRR experiments are conducted in the continuous-flow electrolyzer equipped with 25 cm^2 effective area gas diffusion electrodes (GDE) at ambient pressure and temperature (Supplementary Fig.1). The working electrode (WE, cathode) and counter electrode (CE, anode) are 30 μm stainless steel cloth (SSC) and the PtAu/SSC, respectively (Supplementary Fig.2). Fig.1a, shows the configuration of the continuous-flow reactor and the proton shuttling process for lithium-mediated ammonia synthesis. The proton shuttle can participate in reactions on the formation of lithium nitride (LiN_xH_y) and the generation of ammonia (Fig.1b). Protons are generated through HOR on PtAu anode catalysts[28]. These protons then react with the deprotonated form (B^-, representing base) of the proton shuttle, resulting in the formation of the protonated shuttle (BH) of the proton shuttle. Subsequently, the protonated form diffuses to the cathode, where it protonates lithium nitride, leading to the release of ammonia and the regeneration of the deprotonated shuttle. The specific role and involved reactions of the proton shuttle in the Li-NRR process determine some requirements and design principles for efficient proton shuttles. (1) The proton shuttle should contain a functional group (*e.g.*, -OH and -COOH) that can donate/accept a proton. (2) The proton shuttle should have a proper pK_a in the electrolyte, which strikes a balance between protonation ability and minimizing side reactions, such as hydrogen evolution reaction (HER). If the pK_a of the proton shuttle is too small (*i.e.*, highly acidic), it will undergo a direct reaction with metallic lithium, impeding N_2 activation, or leading to the dominance of the competitive HER reaction on the cathode. Conversely, if the pK_a of the proton shuttle is too large (*i.e.*, less acidic), its protonation ability will be diminished, resulting in inadequate protonation of the nitrogen atoms adsorbed on the lithium[28]. (3) The proton shuttle should possess the capacity to form a functional SEI layer on the cathode, enabling the diffusion of proton and lithium ions through this layer. For example, the EtOH plays an important role in the formation of the SEI layer[28]. (4) The

deprotonated form (B^-) of the proton shuttle should have good electrochemical stability and chemical stability. The high stability of the proton shuttle helps mitigate unwanted side reactions and ensures the overall stability of the operating system. (5) The proton shuttle should exhibit an optimal diffusion rate to effectively control the concentration of available protons on the surface of lithium nitride. Both the steric effect and hydrogen bonding can significantly impact the diffusion rate of the proton shuttle within the electrolyte. (6) The proton shuttle and the Li-NRR system should demonstrate excellent compatibility with each other. For example, the proton shuttle must not poison the HOR catalyst. Due to concerns regarding the poisoning of the anode catalysts, we refrained from testing thiols as proton shuttles in our study.

Based on these design principles for effective proton shuttles, the Li-NRR performance of various categories of proton shuttles, including alcohols, amines, phenols, phosphonium salts, and carboxylic acids, were evaluated in a continuous-flow electrolyzer under the same condition (Fig.1c and Supplementary Table 1). The electrolyte was 1 M lithium tetrafluoroborate ($LiBF_4$) in THF with 37 mM or 50 mM proton shuttles. The ethanol (**2**) (bold numbers refer to Fig.1c), 1-propanol (**3**), and 1-butanol (**4**) exhibited relatively high FE, which is consistent with previous reports[21-23]. Interestingly, a noticeable drop in FE is observed when larger groups are substituted, as evidenced by the comparison between compounds **2** and **6**, as well as **5** and **7**. In contrast, the amines, such as pyridine (**8**) and proton sponge (**11**), have a basic group, but cannot easily donate or abstract a proton. Therefore, amines are bad as shuttles. The phosphonium salts (**16**, $[P_{6,6,6,14}][eFAP]$) was synthesized by ion exchange reaction and confirmed by nuclear magnetic resonance (NMR) spectroscopy (Supplementary Fig.3). To mitigate the influence of oxygen and water on the performance of phosphonium salts, the Li-NRR experiments were conducted within an Ar-filled glovebox[17]. The activity of phosphonium salts (**16** and **17**) was observed to be lower

than that of alcohols, which could be attributed to the difficulty of carrying protons and lower diffusion rate. As anticipated, the acids (**18** and **19**) exhibited lower activity due to their highly acidic nature. Among the various proton shuttles evaluated, phenol (**12**) displayed the highest FE of 72 ± 3% in the Li-NRR process, surpassing that of ethanol. Subsequently, more experiments and discussions will be focused on investigating phenol as a proton shuttle, considering its notable performance in the Li-NRR.

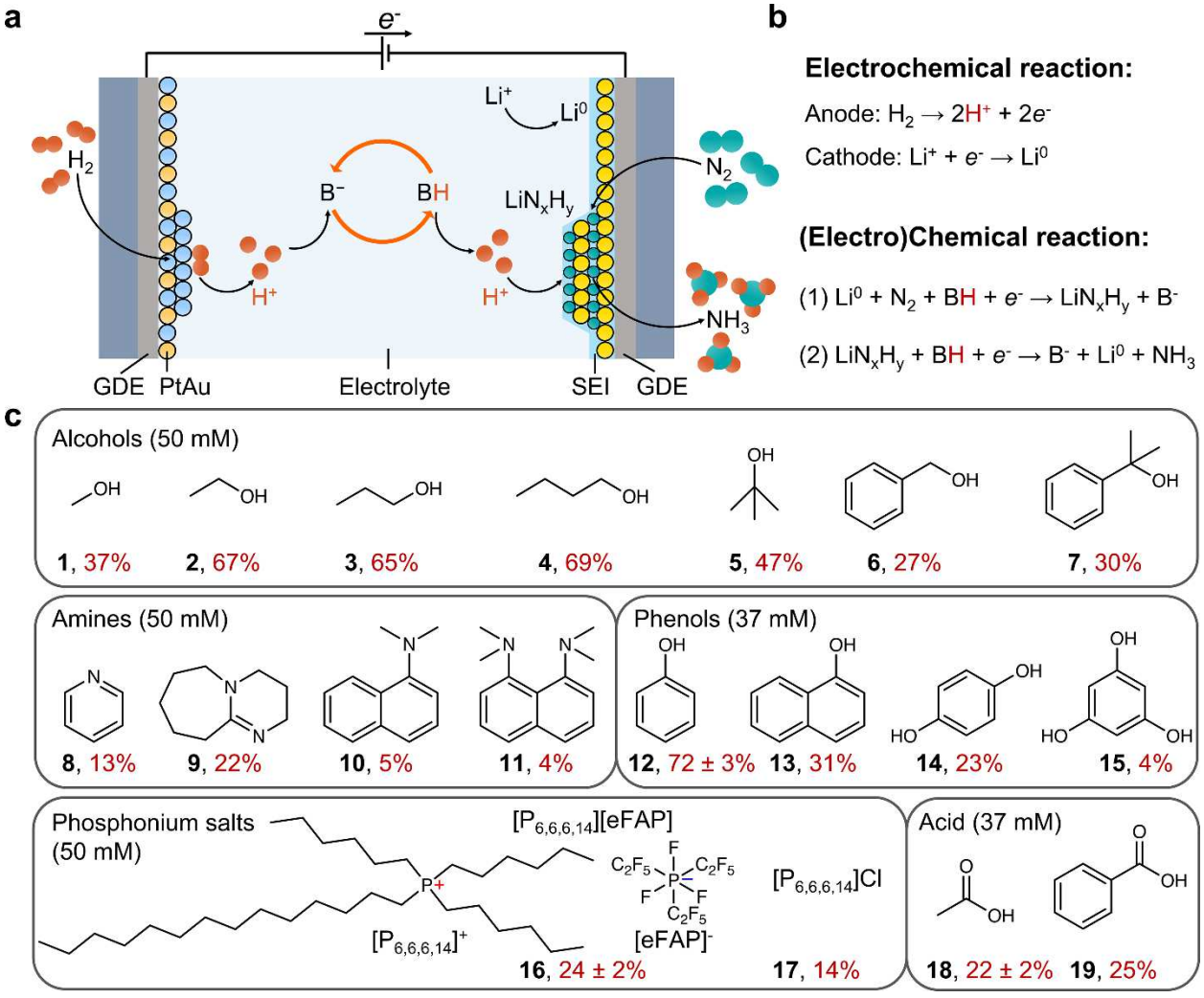

Fig. 1 Proton shuttles screening in a continuous-flow reactor. ***a****, Schematic proton shuttling process for lithium-mediated ammonia synthesis in a continuous-flow electrolyzer.* ***b****, Lithium plating at the cathode and hydrogen oxidation reaction at the anode.* ***c****, Ammonia faradaic*

efficiencies for a variety of proton shuttles. FEs towards ammonia of proton shuttles were determined by passing a total charge of 700 C (over 2.5 h) with the optimal potential cycling (-6 mA cm^{-2} for 1 min and then 0 mA cm^{-2} for 1 min) under the same test conditions. The standard deviation of FE is from at least three independent measurements.

Verification of Phenol as a Proton Shuttle

As found in our previous work, the optimal potential cycling condition entails applying a current density of -6 mA cm^{-2} for 1 min (the corresponding potential denoted deposition potential) and then 0 mA cm^{-2} for 1 min (the corresponding potential denoted resting potential)[28]. The FEs of proton shuttles were obtained by passing a total charge of 700 C under the optimal potential cycling condition. As shown in Fig.2a, the chronopotentiometry (CP) of PhOH exhibited average anode potential and cathode potential values of approximately 0.7 V and 3.6 V versus Pt, respectively. The FE towards ammonia was found to be dependent on the concentration of PhOH, with FE of 72 ± 3% at the optimal concentration of 37 mM (Fig.2b). This concentration dependence arises from the presence of protons within PhOH, which directly influences the available proton concentration in the Li-NRR system (Supplementary Fig.4). In comparison to the absence of a proton shuttle, the ammonia produced using PhOH was predominantly distributed in the gas phase and electrolyte, accounting for over 90% of the total ammonia generated (Fig.2c). During the 1min resting period at the open circuit voltage (OCV), the resting potential of the cathode in the CP curve is expected to increase because of the reaction between the proton shuttle and the cathode surface species. The resting potential in the absence of the proton shuttle was -3 V versus Pt, which can be the benchmark for the resting potential in the presence of the proton shuttle (Supplementary Fig.5). For example, the resting potential with ethanol is -2 V versus Pt, but with acetate acid, it is

-1 V versus Pt due to its highly acidic nature (Supplementary Fig.6 and 7). When comparing compounds **2** and **6**, **5** and **7**, **18** and **19**, as well as **12** and **13**, a higher ratio of ammonia in electrode deposits to a total ammonia (*i.e.*, the proton shuttle cannot protonate LiN_xH_y in time and the LiN_xH_y is accumulated) is observed when proton shuttles are substituted by larger groups (Supplementary Fig.8). This higher ratio could be indicative of a lower protonation ability of the proton shuttle, which is reflected by the resting potential approaching -3 V (*i.e.*, no oscillation) during OCV (Supplementary Fig.5-7).

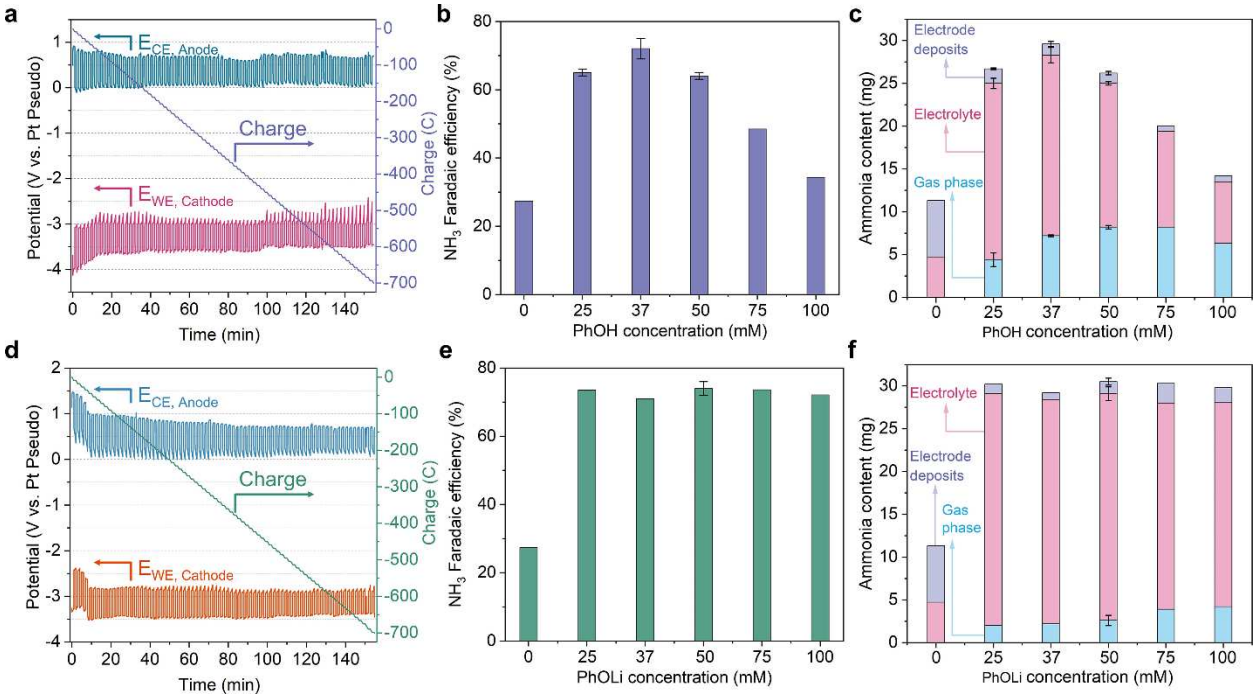

Fig. 2 Performance of Li-mediated ammonia synthesis using phenol or lithium phenoxide as proton shuttles. a, *The chronopotentiometry using phenol as proton shuttles (37 mM).* ***b,*** *Faradaic efficiency changed with varying phenol concentrations.* ***c,*** *The various phenol concentrations affect the distribution of produced ammonia in the electrolyte, gas phase, and electrode deposits.* ***d,*** *The chronopotentiometry using lithium phenoxide as proton shuttles (37 mM).* ***e,*** *Faradaic efficiency changed with varying lithium phenoxide concentrations.* ***f,*** *The various lithium phenoxide concentrations affect the distribution of produced ammonia in the electrolyte, gas phase,*

and electrode deposits. All potentials are without iR correction. The potential cycling condition is -6 mA cm^{-2} for 1 min and 0 mA cm^{-2} for 1 min. All experiments passed a total charge of 700 C at the current density of -6 mA cm^{-2} with the same potential cycling condition. Error bars represent the standard deviation from at least three independent measurements.

To provide further evidence of the proton shuttle's ability to transfer protons in the actual Li-NRR process, we propose a procedure that involves utilizing the deprotonated form (B^-) of the proton shuttle to evaluate its proton transfer capability. Additionally, we suggest employing operando isotope-labelled mass spectrometry (*i.e.*, deuterium oxidation reaction) to confirm that the hydrogen present in the produced ammonia originates from the HOR. Firstly, PhOH was substituted with lithium phenoxide (PhOLi) to evaluate its performance in the Li-NRR process. Fig.2d illustrates the CP of PhOLi, exhibiting that its anode and cathode potentials are consistent with those shown in Fig.2a. During the initial ten minutes of CP (Fig.2d), the anode and cathode potentials were shifted, which can be attributed to the relatively low proton concentration in the early stages. A similar phenomenon was observed using lithium ethoxide (EtOLi) in the Li-NRR process (Supplementary Fig.9). Unlike PhOH, the ammonia FE was independent of the concentration of PhOLi (Fig.2e), which indicated the available proton concentration in the electrolyte was only limited by the current density of HOR. Remarkably, a FE of 74 ± 2% was achieved at a PhOLi concentration of 50 mM, which closely approached the performance achieved at the optimal concentration of PhOH. These results serve as direct evidence that the deprotonated form of PhO^- ions functions as the proton shuttle for proton transfer in the real Li-NRR process. When utilizing PhOLi, the distribution of ammonia in the gas phase is lower compared to using

PhOH (Fig.2f), which could be attributed to the different properties of the solid electrolyte interphase (SEI) layer or electrode deposits.

To reveal the difference in SEI and electrode deposits between the PhOH and PhOLi (Supplementary Fig.10 and 11), flow cell experiments were performed in an Ar-filled glovebox under four conditions — *i.e.*, after a linear sweep voltammetry (LSV) test with either PhOH or PhOLi and after 700 C of CP with either PhOH or PhOLi. The scanning electron microscope (SEM), x-ray diffraction (XRD), and x-ray photoelectron spectrometer (XPS) transfer systems were utilized to avoid exposure to air and moisture (Supplementary Fig.12-14). The SEM images reveal the formation of a dense SEI layer following the LSV test with PhOH, whereas fewer deposits were observed with PhOLi (Supplementary Fig.15). After a total charge of 700 C in the CP test, the cathode surface of PhOLi exhibited an irregular and thicker layer of deposits, while a uniform and thinner layer of deposits was observed when using PhOH (Supplementary Fig.16 and 17). This observation explains the lower distribution of ammonia in the gas phase when PhOLi was utilized as the proton shuttle (Fig.2f). The XRD patterns confirmed the main component of electrode deposits is lithium fluoride (LiF) after 700 C of the CP test with PhOH or PhOLi (Supplementary Fig.18 and 19). The depth-profiling XPS spectra further validated that LiF was the dominant species present in both the SEI and electrode deposits when using either PhOH or PhOLi, aligning with previous findings (Supplementary Fig.20-25)[27,28]. After 700 C of the CP test with PhOH or PhOLi, the N 1s peak at 398 eV is attributed to LiN_xH_y (Supplementary Fig. 24 and 25).

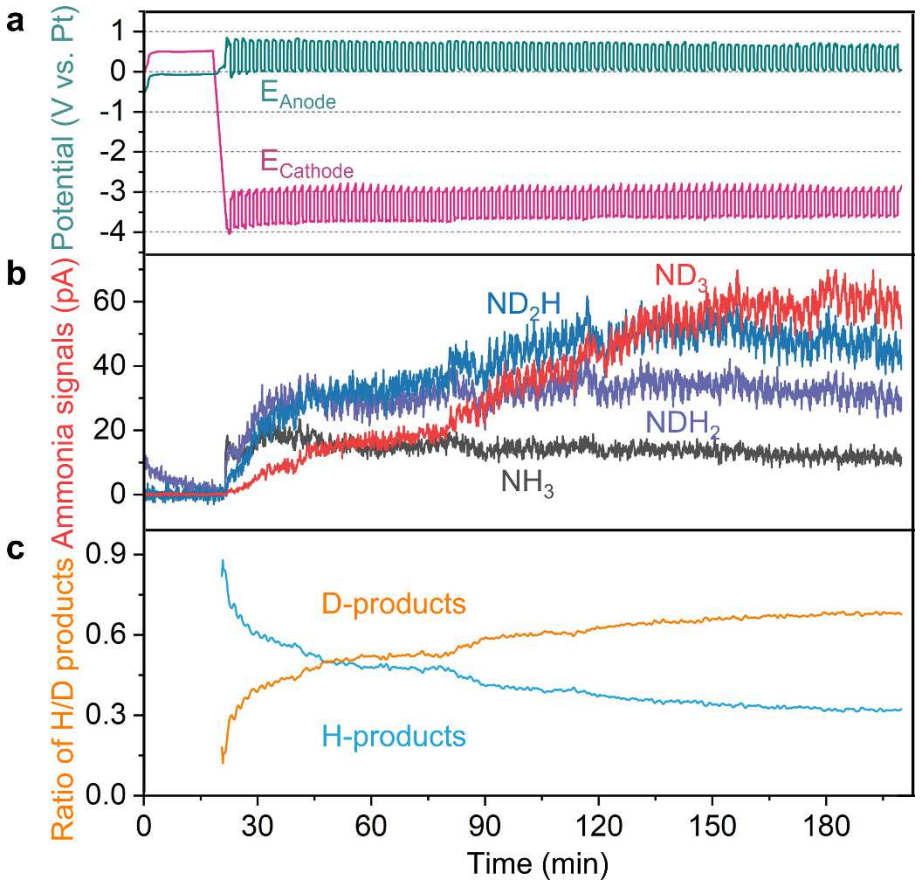

Fig. 3 Operando mass spectrometry of cathodic ammonia gas products with isotope-labelled deuterium using phenol as proton shuttle. a, *The chronopotentiometry using phenol as proton shuttle.* ***b,*** *Measured gas-phase ammonia when the anode occurs deuterium oxidation reaction.* ***c,*** *The corresponding measured relative amounts of D-contained or H-contained ammonia.*

Operando isotope-labelled mass spectrometry is another necessary experiment for the proposed procedure to prove the ability to transfer the proton of the proton shuttle. The operando mass spectrometry was conducted in a continuous-flow reactor, wherein a deuterium (D_2) oxidation reaction occurred at the anode side to generate protons (D^+) to examine whether the proton shuttle (PhOH) can transfer the protons to the cathode products (Fig.3). The products containing deuterium (D) and hydrogen (H) were measured at the cathode side using operando mass

spectrometry (Supplementary Fig.26). Initially, the cathode is surrounded by fresh electrolyte, resulting in a predominance of H-containing products such as NH_3 and NH_2D (Fig.3b). As expected, as the experiment progresses, more and more the D-containing products were generated, eventually leading to a dominance of the fully deuterated ammonia (ND_3) (Fig.3c). Those results unambiguously demonstrate the proton-shuttling capability of PhOH, transferring protons from HOR to the cathode products. At the initial stage, the PhOH is fully protonated with H, resulting in the generation of H-containing products. When the deprotonated form (PhO^-) was formed, PhO^- can be further re-protonated by D^+. Subsequently, the PhOD can protonate the lithium nitrides to generate the D-containing ammonia.

To further elucidate the ability of the deprotonated form (PhO^-) to interact with protons during the Li-NRR process, nuclear magnetic resonance (NMR) spectra of electrolytes were conducted before and after the electrochemistry test (Supplementary Fig.27 and 28). As shown in Fig.4a, the deprotonated form (PhO^-) acts as a proton acceptor, effectively protonating the protons originating from the HOR to form PhOH. Subsequently, the PhOH reacts with LiN_xH_y to release ammonia and regenerate the deprotonated form (PhO^-). The NMR spectra of PhOLi and PhOH before the electrochemistry test are a benchmark for NMR analysis (Fig.4b and Supplementary Fig.29). The slight shift of ^1H NMR peaks of PhOH before and after the electrochemistry test (Supplementary Fig.29) was due to slight differences in the pH (*i.e.*, after test produced ammonia). Quantitative NMR measurements indicate that the amount of PhOH remains almost unchanged after the electrochemistry test (Supplementary Fig.30). This suggests that PhOH is relatively stable under the experimental conditions and does not undergo significant decomposition or consumption during the Li-NRR process. Notably, after the electrochemistry test, almost all of the PhOLi were

observed to convert into PhOH through protonation (Fig.4c). This conversion of PhOLi to PhOH indicates the efficient proton transfer ability of PhOLi during the Li-NRR process. Taken together, the set of experiments conducted, including the examination of the proton transfer capability of PhOLi in the real Li-NRR process, operando isotope-labelled mass spectrometry, and NMR analysis, provide unambiguous evidence of the proton-shuttling capability of PhOH.

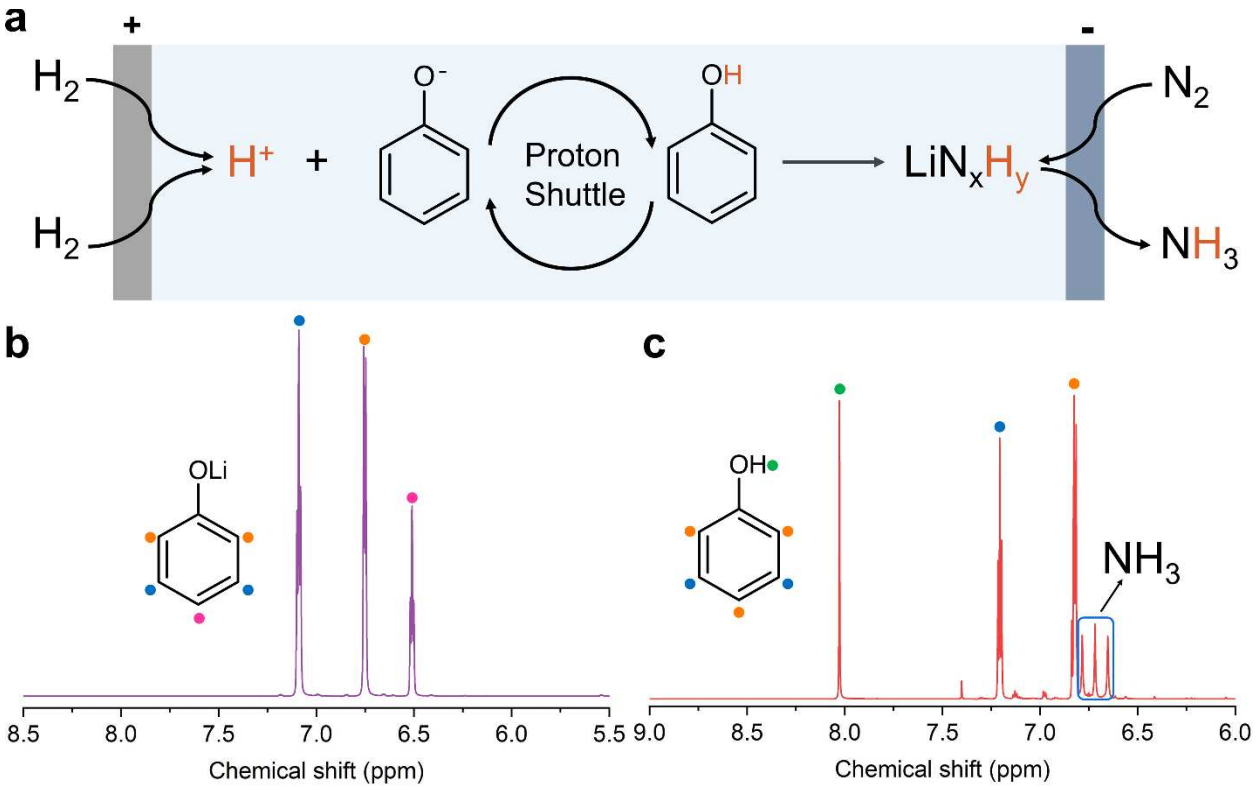

Fig. 4 Demonstration of the ability of phenol for proton shuttling. a, *Schematic for proton shuttling process of phenol in Li-mediated ammonia synthesis.* ***b,*** *The ^{1}H NMR spectra of lithium phenoxide in tetrahydrofuran before the electrochemistry test.* ***c,*** *The ^{1}H NMR spectra of post-reaction electrolytes using lithium phenoxide as proton shuttle after the electrochemistry test (700 C of CP).*

Deprotonated form of proton shuttle as proton buffer

Furthermore, when acetic acid was utilized as the proton shuttle, the FE of ammonia was only 22% ± 2%, primarily due to the enhanced occurrence of the competitive HER (Supplementary Fig.31). When the mixture of PhOLi (37 mM) with acetic acid (37 mM) was employed as the proton shuttle, the FE towards ammonia improved to 31% ± 1% (Supplementary Fig.32). This improvement can be attributed to the proton-buffering capability of PhOLi (*i.e.*, lowers the available proton concentration in the electrolyte), which effectively mitigates the adverse effects of the competitive HER (Supplementary Fig.31).

Stability of deprotonated form for proton shuttle

One key requirement for an efficient proton shuttle is that the deprotonated form of the proton shuttle should demonstrate both excellent electrochemical stability and chemical stability during the Li-NRR process. We selected state-of-the-art EtOH as a reference for comparing stability. Fig.5a and 5b illustrate the deprotonation reactions of EtOH and PhOH, respectively. It is well known that the resonance-stabilized phenoxide ion is more stable than an ethoxide ion[30,31], evidenced by the electrostatic potential maps from density functional theory (DFT) calculations (Fig.5c and 5d), where less negative charge resides on the oxygen atom of phenoxide, compared to ethoxide. When lithium ethoxide (EtOLi) was used as a proton shuttle, the FE achieved was only 26 ± 1% (Supplementary Fig.33), significantly lower than that of PhOLi (74 ± 2%). The lower performance of EtOLi may be attributed to the relatively lower stability of the ethoxide ion compared to the phenoxide ion (Supplementary Fig.30 and 34). The electrochemical stability of EtOH and PhOH was investigated in an aqueous electrolyte (Supplementary Fig.35). The onset and peak oxidation potentials revealed a distinct stability order under the same experimental conditions: PhOH demonstrated superior stability compared to EtOH and THF, a result consistent

with previous studies[32-34]. Notably, the oxidation current density of PhOH was significantly smaller than that of EtOH, indicating excellent electrochemical stability. These findings emphasize the stability of PhOH as an efficient proton shuttle in practical Li-NRR process.

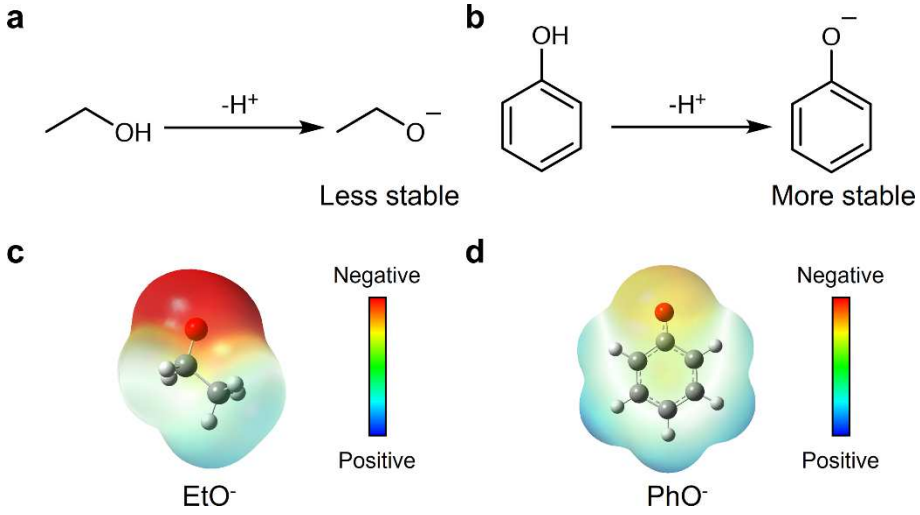

Fig. 5 Stability of deprotonated form for proton shuttles. a, b *Deprotonated reaction of ethanol* ***(a)*** *and phenol* ***(b)****.* ***c, d*** *Electrostatic potential map of ethoxide ion* ***(c)*** *and phenoxide ion* ***(d)****.*

Thermodynamic calculations indicate that, on the cathodic side, all electrochemical steps of NRR are energetically favorable under operation[29], while HOR is highly selective on the PtAu anode depending on whether ethanol or phenol is the shuttle (Supplementary Fig.36). We then employed a mass transport model to simulate the Li-NRR system based on the fact that diffusion of N_2 and H^+ is significantly slower than reaction kinetics, and rate-limiting overall. The model, which is based on the model and extended to include homogeneous reactions in electrolytes[14], is described in detail in SI-Computational methods, showing general consistency with experimental data (Supplementary Fig.37)[4,28], contributing to a reasonable understanding of the volcano-like relationship for proton shuttle concentrations vs. NH_3 selectivity, and a prediction of shifted trend of optimal FE at the balance between N_2 vs. H^+ flux. The latter is dependent on proton shuttle

concentrations and species. In the case of acidic shuttles with a lower pK_a, *e.g.*, acetate acid, the proton is much easier to transport from anode to cathode by protonation and deprotonation, leading to a larger value of proton flux at the same concentration, thereby an increased FE of ammonia in the H^+-limited region and a decreased FE in the N_2-limited region, as shown in Fig.6a. At a specific proton shuttle concentration like our experimental setup, a new volcano plot (Supplementary Fig.38) would be able to elucidate the effects of proton shuttle pK_a.

Accurate evaluation of pK_a in THF is essential to quantify proton shuttle influence. We applied solvent-corrected DFT to benchmark pK_a calculation (Supplementary Fig.39) for a series of alcohols and acids. The calculation outcomes (Supplementary Table 2) show good agreement with the literature and expands the capacity of pK_a datasets in organic solvent[35]. Taking the calculated pK_a into the mass transport model, we found that the single descriptor, pK_a, cannot completely explain proton shuttles' influence on Li-NRR (Supplementary Fig.40). As an example, an exception is phenol and 1-naphthol which have very close pK_a values (29.24 vs. 29.70), but significant difference in NRR FE performance (72% vs. 30%). Considering the size difference between phenol and 1-naphthol, one may posit the size-related diffusivity of the proton shuttle, as the second descriptor for catalytic performance. The synergistic effects of pK_a and diffusivity on the resulting FE are graphically represented by Fig.6b, in which an optimal NH_3 FE would require either acidic but transport-limited proton shuttles or basic but transport-fast shuttles, in agreement with experimental discovery. The trade-off between diffusion and pK_a is a materialization of H^+ flux, still aligning with our original mass transport model[14].

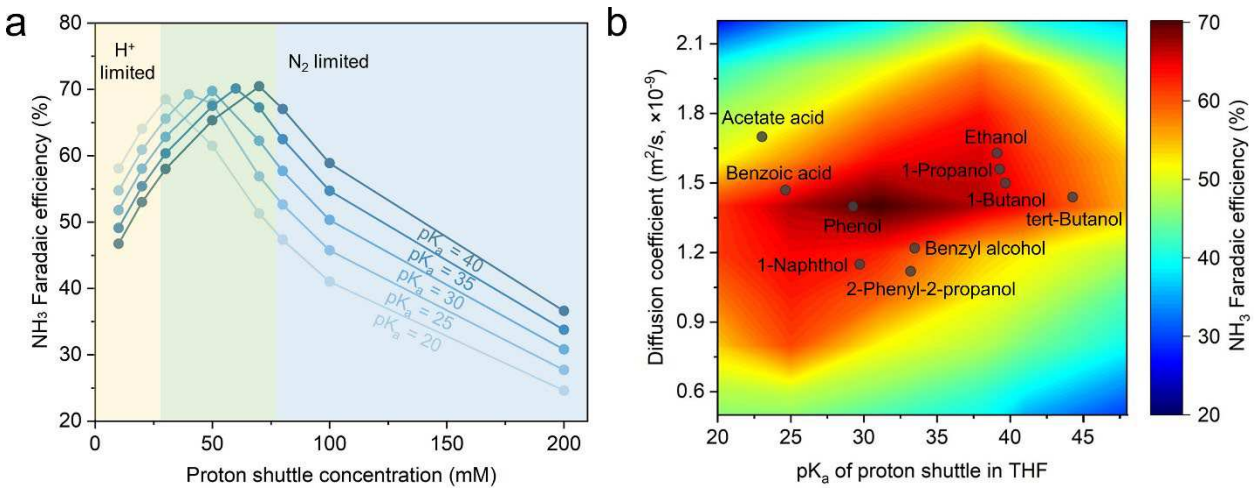

Fig. 6 Dependence of the Li-NRR performance on the pK_a and diffusion coefficient of proton shuttles. a, *A 1D plot of ammonia faradaic efficiency versus concentrations of proton shuttle with different pK_a.* ***b,*** *Heatmap of the predicted ammonia faradaic efficiency as a function of the pK_a of proton shuttle (x-axis) and diffusion coefficient (y-axis).*

Conclusions

In summary, proton shuttle screening has been performed in the practical Li-NRR process with HOR at the anode in a continuous-flow reactor. Proton shuttles play a crucial role in the transfer of protons from the HOR at the anode to the cathode for ammonia synthesis in the Li-NRR process. We propose a general procedure to validate the effectiveness of proton shuttles in the Li-NRR and establish design principles for developing efficient proton shuttles in practical Li-NRR processes. Through this procedure, we demonstrate that the PhOH exhibited excellent proton transfer capabilities and stability in the Li-NRR process. Moreover, the PhOH exhibited an ammonia FE as high as 72 ± 3%, which is among the highest ammonia selectivity achieved in Li-NRR at ambient conditions. The deprotonated form (PhO^-) of the PhOH is proven to act as the primary species responsible for transferring protons during the Li-NRR process. The combination of

theoretical calculations and micro-kinetic modeling provide understanding of the mechanism of proton shuttling in the Li-NRR process. The findings contribute to the understanding of the mechanistic aspects and design principles for efficient proton shuttles in practical Li-NRR applications, ultimately paving the way for the development of sustainable and environmentally friendly ammonia production methods.

References

1. Iriawan, H., *et al.* Methods for nitrogen activation by reduction and oxidation. *Nat. Rev. Method Prime*, **1**, 56 (2021).

2. Chen, J.G., *et al.* Beyond fossil fuel-driven nitrogen transformations. *Science*, **360**, eaar6611 (2018).

3. Fu, X.B., Zhang, J.H., Kang, Y.J. Recent advances and challenges of electrochemical ammonia synthesis. *Chem Catalysis*, **2**, 2590-2613 (2022).

4. Li, K., *et al.* Enhancement of lithium-mediated ammonia synthesis by addition of oxygen. *Science*, **374**, 1593-1597 (2021).

5. Suryanto, B.H.R., *et al*. Challenges and prospects in the catalysis of electroreduction of nitrogen to ammonia. *Nat. Catal.*, **2**, 290-296 (2019).

6. Qing, G., *et al.* Recent Advances and Challenges of Electrocatalytic N_2 Reduction to Ammonia. *Chem. Rev.*, **120**, 5437-5516 (2020).

7. Westhead, O., *et al.* Near ambient N_2 fixation on solid electrodes versus enzymes and homogeneous catalysts. *Nat. Rev. Chem.*, **7**, 184-201 (2023).

8. Singh, A.R., *et al.* Electrochemical Ammonia Synthesis—The Selectivity Challenge. *ACS Catal.*, **7**, 706-709 (2017).

9. Andersen, S.Z., *et al.* A rigorous electrochemical ammonia synthesis protocol with quantitative isotope measurements. *Nature*, **570**, 504-508 (2019).

10. Choi, J., *et al.* Identification and elimination of false positives in electrochemical nitrogen reduction studies. *Nat Commun*, **11**, 5546 (2020).

11. F. Fichter, P.G., H. Erlenmeyer. Elektrolytische Bindung von komprimiertem Stickstoff bei gewöhnlicher Temperatur. *Helv. Chim. Acta*, **13**, 1228-1236 (1930).

12. Tsuneto, A.*, et al.* Efficient Electrochemical Reduction of N_2 to NH_3 Catalyzed by Lithium. *Chem. Lett.*, 851-854 (1993).

13. Tsuneto, A.*, et al.* Lithium-Mediated Electrochemical Reduction of High-Pressure N_2 to NH_3. *J. Electroanal. Chem.*, **367**, 183-188 (1994).

13. Lazouski, N.*, et al.* Understanding Continuous Lithium-Mediated Electrochemical Nitrogen Reduction. *Joule*, **3**, 1127-1139 (2019).

14. Andersen, S.Z.*, et al.* Increasing stability, efficiency, and fundamental understanding of lithium-mediated electrochemical nitrogen reduction. *Energy. Environ. Sci.*, **13**, 4291-4300 (2020).

15. Lazouski, N.*, et al.* Non-aqueous gas diffusion electrodes for rapid ammonia synthesis from nitrogen and water-splitting-derived hydrogen. *Nat. Catal.*, **3**, 463-469 (2020).

16. Cai, X.Y.*, et al.* Lithium-mediated electrochemical nitrogen reduction: Mechanistic insights to enhance performance. *iScience*, **24**, 103105 (2021).

17. Suryanto, B.H.R.*, et al.* Nitrogen reduction to ammonia at high efficiency and rates based on a phosphonium proton shuttle. *Science*, **372**, 1187-1191 (2021).

18. Li, K.*, et al.* Increasing Current Density of Li-Mediated Ammonia Synthesis with High Surface Area Copper Electrodes. *ACS Energy Lett.*, **7**, 36-41 (2022).

19. Cai, X.Y.*, et al.* Membrane electrode assembly design for lithium-mediated electrochemical nitrogen reduction. *Energy. Environ. Sci.*, DOI: 10.1039/D3EE00026E (2023).

20. Sazinas, R.*, et al.* Oxygen-Enhanced Chemical Stability of Lithium-Mediated Electrochemical Ammonia Synthesis. *J. Phys. Chem. Lett.*, **13**, 4605-4611 (2022).

21. Krishnamurthy, D.*, et al.* Closed-Loop Electrolyte Design for Lithium-Mediated Ammonia Synthesis. *ACS Cent. Sci.*, **7**, 2073-2082 (2021).

22. Lazouski, N., *et al.* Proton Donors Induce a Differential Transport Effect for Selectivity toward Ammonia in Lithium-Mediated Nitrogen Reduction. *ACS Catal.*, **12**, 5197-5208 (2022).

23. Du, H.L., *et al.* The chemistry of proton carriers in high-performance lithium-mediated ammonia electrosynthesis. *Energy. Environ. Sci*, **16**, 1082-1090 (2023).

24. Steinberg, K., *et al.* Imaging of nitrogen fixation at lithium solid electrolyte interphases via cryo-electron microscopy. *Nat. Energy*, **8**, 138-148 (2023).

25. Gao, L.F., *et al.* Domino Effect: Gold Electrocatalyzing Lithium Reduction to Accelerate Nitrogen Fixation. *Angew. Chem. Int. Ed.*, **60**, 5257-5261 (2021).

26. Du, H.L., *et al.* Electroreduction of nitrogen with almost 100% current-to-ammonia efficiency. *Nature*, **609**, 722-727 (2022).

27. Li, S., *et al.* Electrosynthesis of ammonia with high selectivity and high rates via engineering of the solid-electrolyte interphase. *Joule*, **6**, 2083-2101 (2022).

28. Fu, X., *et al.* Continuous-flow electrosynthesis of ammonia by nitrogen reduction and hydrogen oxidation. *Science*, **379**, 707-712 (2023).

29. Schwalbe, J.A., *et al.* A Combined Theory-Experiment Analysis of the Surface Species in Lithium-Mediated NH_3 Electrosynthesis. *ChemElectroChem*, **7**, 1542-1549 (2020).

30. Went, C. in *Ionic Organic Mechanisms*, 58-78 (Palgrave, 1986).

31. McMurry, J. E. in *Fundamentals of Organic Chemistry*, 261-262 (Cengage Learning, 2010).

32. Avgousti, C., *et al.* The electrochemical oxidation of tetrahydrofuran in sulphuric acid solution. *Electrochim. Acta.*, **44**, 3295-3301 (1999).

33. Zhang, L.Y., *et al.* Ultrasmall and uniform Pt_3Au clusters strongly suppress Ostwald ripening for efficient ethanol oxidation. *Electrochem. Commun.*, **84**, 1-5 (2017).

34. de Souza, R.B.A., Ruotolo, L.A.M. Phenol Electrooxidation in Different Supporting Electrolytes Using Boron-Doped Diamond Anodes. *Int. J. Electrochem. Sci.*, **8**, 643-657 (2013).

35. Kutt, A.*, et al.* pK_a values in organic chemistry - Making maximum use of the available data. *Tetrahedron Lett.*, **59**, 3738-3748 (2018).

Methods

Preparation of cathode electrodes.

The 316 stainless steel cloth (SSC, McMaster-Carr, 500 x 500 mesh, pore size of 30 μm) was used as the cathode electrodes for the electrochemical ammonia synthesis test. Before use, the SSC was cleaned with acetone and ethanol 3 times. The treated SSC was dried in the vacuum oven for further use.

Preparation of anode electrodes.

The PtAu/SSC was prepared by electrodeposition as previously described. Brief description for the electrodeposition, SSC with a pore size of 5 μm (McMaster-Carr, 325 x 2300 mesh) was used as the working electrode, and two Pt mesh electrodes (Goodfellow, 1.5 cm×1.5 cm, 99.9 %) were electrically connected and used as a split counter electrode. The 10 mM $H_2PtCl_6 \cdot 6H_2O$ (Sigma Aldrich, ACS reagent) with 10 mM $HAuCl_4 \cdot 3H_2O$ (Sigma Aldrich, 99%) in 3 M H_2SO_4 (Sigma Aldrich, 99.999%) solution was used as the electrolyte for electrodepositing PtAu/SSC. A current density of -0.2 A/cm^2 was applied for 2 min in which rigorous hydrogen evolution and metal deposition took place at the same time, leading to high surface area structures of PtAu on the SSC. After the electrodeposition, the electrodes were rinsed in EtOH and ultra-pure water (18.2 MΩ resistivity, Millipore, Synergy UV system) several times to remove residual electrolytes.

Electrochemical experiments

The electrochemical ammonia synthesis was performed in a three-chamber flow cell (Supplementary Fig.1). More details have been reported in our previous study[28]. The effective electrode area of the flow cell was 25 cm^2. The central electrolyte chamber is made of polyetheretherketone (PEEK, THF-resistant materials). The N_2 (5.0, Air Liquide) and H_2 (5.0, Air

Liquide) gas flow rates were controlled using a mass flow controller (Brooks Instrument) and set to 75 sccm. The N_2 and H_2 used in the experiments were cleaned by purifiers (NuPure) to reduce labile N-containing compounds to parts per trillion by volume (ppt-v) level. Before each experiment, the flow cell parts were boiled in ultra-pure water for 3 h and dried overnight at 100 °C in an oven. The cleaned SSC (500 x 500 mesh, thickness: 30 μm) was used as the working electrode (WE, cathode). As-prepared PtAu/SSC was used as the counter electrode (CE, anode). The pseudo reference electrode (RE) was a Pt wire (Goodfellow, 99.99 %, diameter: 0.5 mm). Before electrochemical tests, the Pt wire was flame-annealed.

The $LiBF_4$ (Sigma Aldrich, ≥ 98 %, anhydrous) was dried at 120 ºC for 48 h in a vacuum oven before use. Ethanol (Honeywell, anhydrous) was dried with 3 Å molecular sieves. Electrolyte solution consisted of 1.0 M $LiBF_4$ in tetrahydrofuran (THF, anhydrous, >99.9 %, inhibitor-free, Sigma Aldrich) and 0-100 mM proton shuttles and was prepared in an argon-filled glovebox. A syringe pump (World Instruments) was used to control the flow rate of the electrolytes at 1.0 ml/min. The syringe (Trajan Scientific and Medical, 100 ml) consisted of a borosilicate glass tube and a PTFE plunger (Gas tight). 1 mM of HCl (Sigma Aldrich, Suprapur) aqueous solution was used to control the back pressure and trap the gas-phase ammonia. The gas outlet back pressure of the flow cell was modulated by a 10.5 centimeters 1 mM of HCl solution column (50 mL), which leads to a pressure gradient of 15 mbar between the gas inlet and outlet of the flow cell. Before the injection of electrolyte into the electrolyte chamber, the purified N_2 and H_2 (75 sccm) were introduced into the empty assembled flow cell for at least 30 min. Afterward, the electrolyte solution was injected into the cell in N_2 and H_2 atmospheres.

The electrochemistry experiments were conducted using a BioLogic Potentiostat (VMP2). The resistance between the WE and RE was measured using the potentiostatic electrochemical impedance spectroscopy (PEIS) and the current interrupt technique. The linear sweep voltammetry (LSV) was recorded from the open-circuit voltage (OCV) until lithium plating is clearly seen. Subsequently, chronopotentiometry (CP) was measured with potential cycling. The potential cycling refers to that -6 mA/cm^2 (the corresponding potential denoted *deposition potential*) was applied for 1 min and then 0 mA/cm^2 (the corresponding potential denoted *resting potential*) for 1 min. 700 C of charge was passed for each experiment to determine the ammonia Faradaic efficiency (FE). We note that all experiments were conducted at room temperature and 1 bar pressure. Typically, flow cell experiments were performed in a fume hood. For analysis of the

electrode deposits on the working electrode, the flow cell was run in an Ar-filled glovebox. As the phosphonium salts are sensitive to the water content, using phosphonium salts as proton shuttle experiments were run in an Ar-filled glovebox. The water content of the electrolyte was measured by Karl Fischer Titration (831 KF Coulometer and 728 Stirrer, Metrohm). Before the electrochemistry test, the water content in the electrolyte with phosphonium salts is about 15-21 ppm. When the experiment finished, total NH_3 production was quantified from the (1) gas-phase NH_3 trapped in 1 mM of HCl, (2) NH_3 trapped in the electrolyte, and (3) NH_3 trapped in the electrode deposits. Typically, 120-130 ml of ultra-pure water was used to dissolve the electrode deposits to release trapped NH_3. We note that H_2O can react with N-containing compounds (*e.g.* LiN_xH_y) in the electrode deposits to produce NH_3.

THF, EtOH, and PhOH oxidation experiments in aqueous electrolyte

A good proton shuttle should have high electrochemical stability during the Li-RR process. To evaluate the electrochemical stability of THF, EtOH, and PhOH on the PtAu anode catalysts, the oxidation experiments in an aqueous electrolyte were carried out in a custom-made three-electrode glass cell using the rotating disk electrode method. The Hg/Hg_2SO_4 reference electrode was calibrated before the electrochemistry test. A Pt wire was used as a counter electrode. The working electrode (PtAu/Ti) was obtained from electrodeposited PtAu on a titanium stub (ϕ = 5 mm, 0.196 cm^2). To prepare the PtAu/Ti electrode, an electrolyte of 10 mM $H_2PtCl_6 \cdot 6H_2O$ (Sigma Aldrich, ACS reagent) with 10 mM $HAuCl_4 \cdot 3H_2O$ (Sigma Aldrich, 99%) in 3 M H_2SO_4 (Sigma Aldrich, 99.999%) was used. A current density of -1 A/cm^2 was applied for 2 min in which rigorous hydrogen evolution and metal deposition took place at the same time with 2500 revolutions per minute. The cyclic voltammetry (CV) curve was recorded between 0 and 1.2 V vs RHE at 50 mV/s in Ar-saturated 0.1 M H_2SO_4. The THF, EtOH, and PhOH oxidation activity was evaluated in Ar-saturated 0.1 M H_2SO_4 with 0.1 M THF or 0.1 M EtOH or 0.1 M PhOH electrolyte with a scan rate of 50 mV/s.

Quantification of ammonia

Ammonia production was quantified using ion chromatography (IC, Metrohm) with an autosampler. The materials of the connection tubes, pressure screws, capillaries, and injection needles were PEEK or PTFE (THF-resistant materials). The IC could measure THF-containing

samples that were diluted with ultra-pure water. The IC detection system is a conductivity detector. The cation column (Metrosep C6) was used as a high-capacity separation column. The Metrosep C6 column material was silica gel with carboxyl groups. The eluent (mobile phase) was 3.3 mmol/L HNO_3 (Sigma Aldrich, Suprapur) solution with 10 vol.% acetone (Sigma Aldrich, ≥ 99.9%). The eluent flow rate was 0.9 ml/min. Before use, the eluent was degassed for 30 min to prevent gas bubbles in the high-pressure pump. For the IC measurements, a 20 µl volume of the sample was injected and measured for 20 min. As THF-containing electrolytes could damage the IC and a high concentration of calcium ions could cause adsorption saturation of the column, the electrolyte was diluted 10-100 times with ultra-pure water. The dilution factor depends on the specific experiment and the expected amount of ammonia produced. To protect the cation column, if the sample or diluted sample contains visible particles, it was pre-treated by a filter syringe with a PTFE filter membrane (Whatman Puradisc, 0.45 µm) to remove the particles before testing IC. Based on the IC settings and conditions, the retention time for the standard cation solution (Sigma Aldrich) was: 6.48 min for Li^+, 8.96 min for Na^+, and 15.32 min for K^+. The retention time of NH_4^+ was 10.60 min. Ammonium chloride (Sigma Aldrich, 99.998%) solution was used to make the NH_3 calibration curve. The reliability of the IC method was verified by the colorimetric indophenol method, previously described[28].

Computational methods

Full computational simulation details are provided in the Supplementary Information.

Acknowledgments

We gratefully acknowledge the funding by Villum Fonden, part of the Villum Center for the Science of Sustainable Fuels and Chemicals (V-SUSTAIN grant 9455), Innovationsfonden (E-ammonia grant 9067-00010B), and the European Research Council (ERC) CLUNATRA under the European Uanion's Horizon 2020 research and innovation program (grant agreement no. 741860). X.F. was supported under the MSCA European Postdoctoral Fellowships (Electro-Ammonia Project 101059643).

Author contributions

Conceptualization: X.F., A.X., J.K.N., I.C.

Data curation: X.F., A.X., J.B.P., S.L., R.S., M.S.

Formal Analysis: X.F., A.X., J.B.P., S.L.

Investigation: X.F., A.X., S.L., M.S.

Methodology – Equipment design: X.F., M.S., J.B.P., S.Z.A.

Visualization: X.F., A.X.

Supervision: J.K., P.C.K.V., J.K.N., I.C.

Writing – original draft: X.F., A.X.

Writing – review and editing: X.F., A.X., S.L., Y.Z., N.H.D., J.B.V.M., J.K., P.C.K.V., J.K.N., I.C.

Competing interests

The authors declare no competing interests.

Additional information

Supplementary information is available for this paper at

Correspondence and requests for materials should be addressed to J.K.N or I.C.

Supplementary Files

This is a list of supplementary files associated with this preprint. Click to download.

- PhOHSI.pdf